47. A. P. Marscher and J. J. Broderick, *ibid.* **255**, L11 (1982).
48. L. Maraschi, G. Ghisellini, A. Celotti, in *Testing the AGN Paradigm*, S. S. Holt, S. G. Neff, C. M. Urry, Eds. (American Institute of Physics, New York, 1992), p. 439.
49. C. D. Dermer and R. Schlickeiser, in preparation.
50. F. Melia and A. Königl, *Astrophys. J.* **340**, 162 (1989).
51. C. D. Dermer, R. Schlickeiser, A. Mastichiadis, *Astron. Astrophys.* **256**, L27 (1992).
52. ______, in *The Compton Observatory Science Workshop*, C. R. Shrader, N. Gehrels, B. Dennis, Eds. (NASA Scientific and Technical Information Program, Washington, DC, 1992), pp. 328–334.
53. R. Kinzer, W. Johnson, J. Kurfess, *Astrophys. J.* **222**, 370 (1978).
54. V. Schönfelder, F. Graml, F. P. Penningsfeld, *ibid.* **240**, 330 (1980).
55. J. I. Trombka *et al.*, *ibid.* **212**, 925 (1977).
56. D. J. Thompson and C. E. Fichtel, *Astron. Astrophys.* **109**, 352 (1992).
57. F. W. Stecker, *Astrophys. J.* **212**, 60 (1977).
58. G. F. Bignami, C. E. Fichtel, R. C. Hartman, D. J. Thompson, *ibid.* **232**, 649 (1979).
59. P. C. Gregory and J. J. Condon, *Astrophys. J. Suppl. Ser.* **75**, 1011 (1991).
60. M. A. Abramowicz, in *Extragalactic Radio Sources: from Beams to Jets*, in press.
61. A. Y. S. Cheng and S. L. O'Dell, *Astrophys. J.* **251**, L49 (1981).
62. M. Punch *et al.*, *Nature*, **358**, 477 (1992).
63. S. Garrington, *ibid.* **355**, 771 (1992).
64. J. A. Zensus, L. B. Baath, M. H. Cohen, G. D. Nicolson, *ibid.* **334**, 410 (1988).
65. Comments from and discussions with C. D. Impey, C. E. Fichtel, R. C. Hartman, G. Kanbach, J. D. Kurfess, A. P. Marscher, J. R. Mattox, and D. J. Thompson are gratefully acknowledged. The work of C.D.D. is supported by the Gamma Ray Observatory Guest Investigator Program through NASA grant NAG 5-1547.

Galileo Encounter with 951 Gaspra: First Pictures of an Asteroid

M. J. S. Belton, J. Veverka,* P. Thomas, P. Helfenstein, D. Simonelli, C. Chapman, M. E. Davies, R. Greeley, R. Greenberg, J. Head, S. Murchie, K. Klaasen, T. V. Johnson, A. McEwen, D. Morrison, G. Neukum, F. Fanale, C. Anger, M. Carr, C. Pilcher

Galileo images of Gaspra reveal it to be an irregularly shaped object (19 by 12 by 11 kilometers) that appears to have been created by a catastrophic collisional disruption of a precursor parent body. The cratering age of the surface is about 200 million years. Subtle albedo and color variations appear to correlate with morphological features: Brighter materials are associated with craters especially along the crests of ridges, have a stronger 1-micrometer absorption, and may represent freshly excavated mafic materials; darker materials exhibiting a significantly weaker 1-micrometer absorption appear concentrated in interridge areas. One explanation of these patterns is that Gaspra is covered with a thin regolith and that some of this material has migrated downslope in some areas.

On 29 October 1991, the Galileo spacecraft flew past 951 Gaspra at a distance of 1600 km and obtained the first close-up views of an asteroid. Because Galileo's high-gain antenna has not yet been deployed, it was planned to play back all of the Gaspra data to Earth using the smaller, low-gain antenna in November 1992 when the spacecraft returns for its final Earth flyby on its way to Jupiter. However, analysis of telemetry and optical navigation pictures taken during the weeks before encounter demonstrated that knowledge of the spacecraft and asteroid geometry had reached such high precision that the asteroid could be located in individual frames of the Solid State Imaging (SSI) camera. As a result, it was feasible to play back the relevant portions of four images at the available 40 bits per second data rate in early November 1991. These four images were taken in four different spectral bands (0.40, 0.56, 0.89, and 0.99 μm) within an interval of 25 s and represent the highest spatial resolution color data gathered by Galileo during its 8-km/s flyby. They were obtained at an average range of 16,065 km some 36 minutes before closest encounter. In this article we summarize the major conclusions about the current state and past evolution of Gaspra that can be inferred from these data.

M. J. S. Belton is with the National Optical Astronomy Observatories, Tucson, AZ 85719.
J. Veverka, P. Thomas, P. Helfenstein, D. Simonelli are in the Department of Astronomy, Cornell University, Ithaca, NY 14853.
C. Chapman is with the Planetary Science Institute, Tucson, AZ 85719.
M. E. Davies is with RAND, Santa Monica, CA 90406.
R. Greeley is in the Department of Geology, Arizona State University, Tempe, AZ 85287.
R. Greenberg is with the Lunar and Planetary Laboratory, University of Arizona, Tucson, AZ 85721.
J. Head and S. Murchie are in the Department of Geology, Brown University, Providence, RI 02912.
K. Klaasen and T. V. Johnson are with the Jet Propulsion Laboratory, California Institute of Technology, Pasadena, CA 91109.
A. McEwen is with the U.S. Geological Survey, Flagstaff, AZ 86001.
D. Morrison is with the NASA/Ames Research Center, Moffett Field, CA 94035.
G. Neukum is with the Deutsche Forschungsanstalt für Luft und Raumfahrt, 8031 Oberpfaffenhofen, Federal Republic of Germany.
F. Fanale is with the Institute of Geophysics, University of Hawaii, Honolulu, HI 96822.
C. Anger is with the Institute for Space and Terrestrial Science, Concord, Ontario, Canada L4K 3C8.
M. Carr is with the U.S. Geological Survey, Menlo Park, CA 94025.
C. Pilcher is with NASA Headquarters, Washington, DC 20546.

*To whom correspondence should be addressed.

Among the more than 5000 numbered asteroids, 951 Gaspra is a relatively small, highly elongated, object (*1, 2*) with an average radius of about 7 km (*3*). It orbits near the inner edge of the main asteroid belt (semimajor axis of 2.21 astronomical units) in the so-called Flora region. Its spectral properties observed from Earth place it in the S taxonomic class, the most common asteroid type in the inner half of the asteroid belt (*4, 5*). Surfaces of S-type asteroids are thought to be composed of varying proportions of olivine and pyroxene and iron-nickel metal, but there is debate about whether the S-asteroids are the parent bodies of the common ordinary chondrite meteorites or whether they are geochemically differentiated bodies in which metal segregated from silicates during an early episode of heating and are the sources of the stony-iron meteorites (*6*). A prime goal of Galileo's encounter with Gaspra and the possible encounter in 1993 with another S-type asteroid, 243 Ida, is to study two diverse S-types. Ground-based reflectance spectra show that Gaspra is an unusually red, olivine-rich, S-type, suggesting that it is possibly a fragment of a differentiated body, whereas Ida is a more likely candidate for an ordinary chondrite parent body (*1, 7, 8*).

The Flora region is densely populated with small, S-type asteroids, generally thought to be the fragments of one or more larger precursor asteroids smashed by catastrophic collisions. Gaspra ought to be a collisional fragment, because rocky objects of its size have model lifetimes against collisional destruction much shorter than the age of the solar system (*9–11*).

Appearance, Size, and Shape

Gaspra is revealed to be an irregularly shaped body with a conspicuously cratered surface, but one with a scarcity of craters larger than about 1.5 km in diameter. There are also hints of generally linear features at the limit of resolution (164 m per pixel; phase angle = 39°). The illuminated portion of Gaspra (Fig. 1), about 16 by 12 km, displays an aspect consistent with Earth-based predictions based on light curve analyses, which yield a spin period of 7.04 hours and a spin axis pointing in the

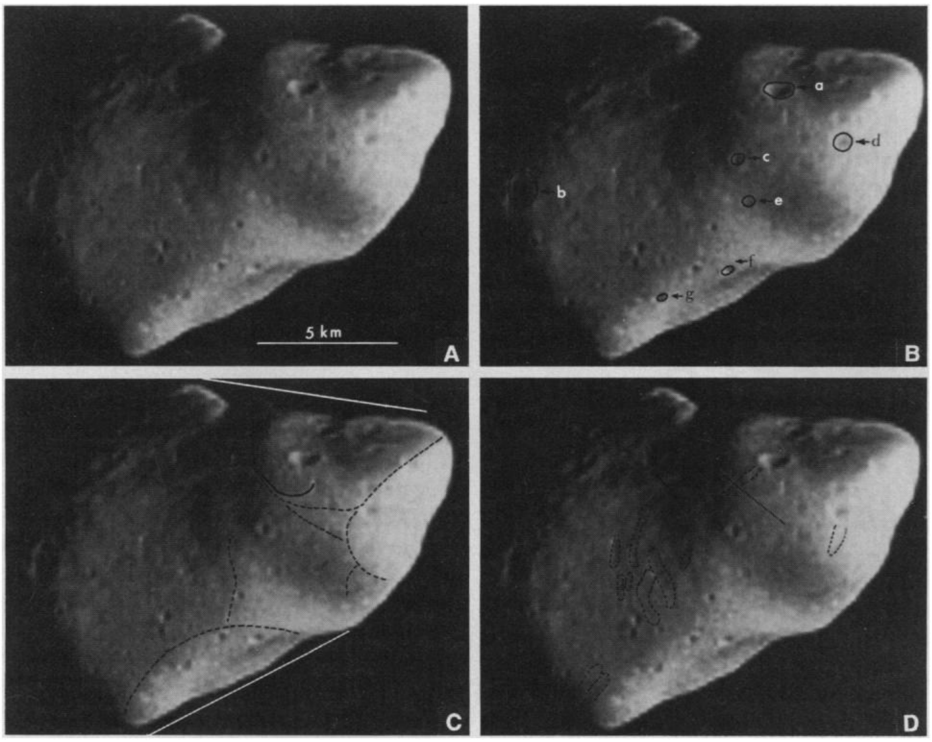

Fig. 1. (**A**) Galileo green image (1073160.65). Phase angle is 39°; resolution is 164 m per pixel. The sun direction is toward the right (compare with Fig. 2). (**B**) Outline of several prominent craters discussed in text. (**C**) Outline of some major ridges that define Gaspra's shape. Also indicated are two large limb concavities. (**D**) Location of some elongated depressions and lineations seen near the limit of resolution.

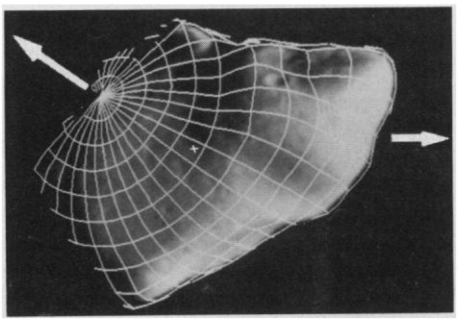

Fig. 2. Galileo violet image (1073160.78) with superimposed shape model. Grid spacing is 10°. Approximate pole location shown is from Earth-based light curve observations (*2*), which suggest a prograde rotation for Gaspra (counterclockwise in this view) with a period of 7.04 hours. The white cross marks the projection of the model's center. The arrow at right points to the sun.

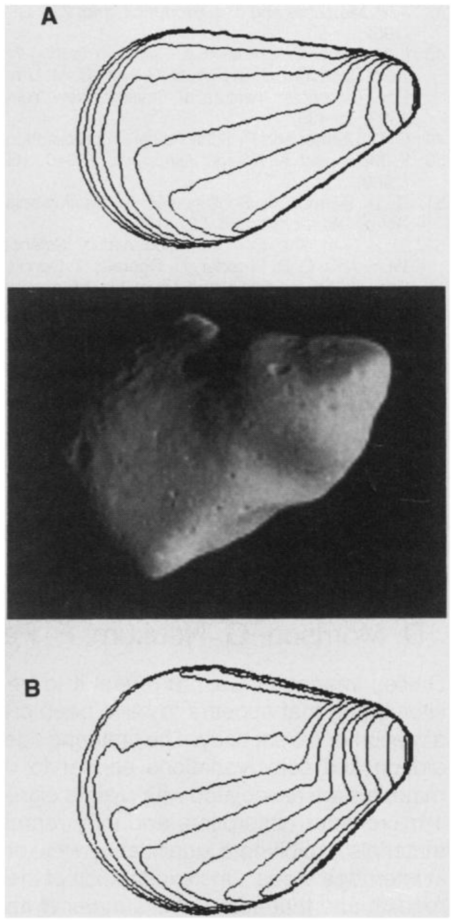

Fig. 3. Alternate "cone model" of Gaspra. The contours, included to give an idea of the shape, are isophotes calculated using Hapke parameters determined by Mottola *et al.* (*13*) in an investigation of the ground-based light curve. Small kinks in the isophotes are artifacts induced at the join between the hemispheric ends and the truncated cone. In (**A**), the model is consistent with the observed light curve and the spin vector determined by Magnusson *et al.* (*2*); it clearly gives an excellent account of the Galileo image. In (**B**), the spin pole has been moved 19° toward the west to give an improved account of the height/breadth aspect ratio seen in the image. The sun is toward the right.

direction right ascension = 9° declination = +28° (*2*). The asteroid's shape is defined by smooth, gently curving surfaces that intersect along ridges (Fig. 1C). Two large concavities dominate the limb; both have chords of about 8.5 km, or about 1.2 times the mean radius of Gaspra.

We modeled the asteroid's shape (Fig. 2) by interactively matching the observed limb and terminator and using the pole orientation determined by Magnusson *et al.* (*2*) from the analysis of observed light curves. Appropriate modifications to the modeled shape were made to agree with the topography inferred from shading observed across the image. The dimensions of the model are 18.7 by 12 by 11 km. Because only 30% of the surface is in view and because there is no useful stereoscopic coverage, the model is not unique. Although knowledge of Gaspra's detailed shape and precise volume remains uncertain, the model is adequate for comparison with other objects, and provides the initial information on local slopes needed for analysis of the photometric and color data.

An alternative estimate of Gaspra's shape can be obtained from available light curve information (*1*, *2*) and checked for consistency with the Galileo images. The asymmetric nature of Gaspra's light curve (distinctly uneven and variable minima) shows that Gaspra must be elongate and that one end is probably larger than the other. A cone model (Fig. 3) in which two hemispherical ends are joined by a tapering cylindrical section provides an excellent fit to the light curve data (*13*) and to the Galileo images. The dimensions of the cone model are scaled so that the spherical ends have diameters that are 0.25 and 0.63 of the overall length. According to this model, Galileo would have viewed approximately the pointed end of Gaspra. The remarkably good consistency of this analysis with the expectations based on the Earth-based predictions (*2*) suggests that the calculated rotation phase and period are essentially correct but that the pole direction may require a small adjustment (Fig. 3). A thorough analysis must await the receipt of images showing other aspects of the asteroid.

On the basis of the above model, Gaspra has a mean radius (R_m) of about 7 km, placing its size between those of the two small satellites of Mars: Deimos (R_m = 6.2 km) and Phobos (11.1 km) (*3*). In Fig. 4 we compare Gaspra's shape with those of other small bodies using as a simple measure of

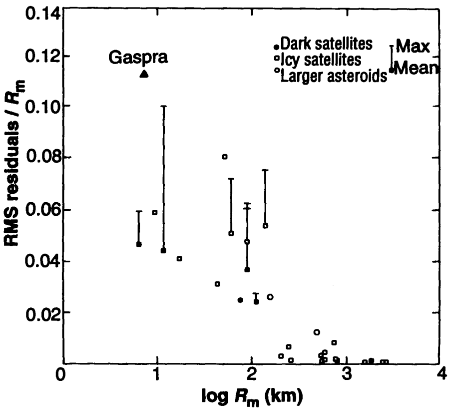

Fig. 4. Comparison of Gaspra's limb roughness with those of other small bodies. RMS is the root-mean-square deviation of an observed limb profile from the best elliptical fit. For some objects, in addition to the mean values, we also plot the maximum observed. R_m is the object's mean radius. Most of the data are from Thomas (*14*); the information on asteroids (other than Gaspra) is derived from observations of stellar occultations (*48*).

roughness the root-mean-square (RMS) residuals of the best-fit ellipse to limb coordinates as a fraction of the mean radius (*14*). For Gaspra the RMS residual is 0.83 km, or about 11% of the mean radius. Small rocky and icy satellites have typical values of 4 to 6%; the maximum observed is 10%, for one particular aspect of Phobos. Gaspra is the most irregular object yet observed, although its shape does fit the general trend, indicated by Fig. 4, that small bodies tend to be more irregular than larger ones. That Gaspra was far from spherical was already known from ground-based observations of the asteroid's large light curve amplitude, which reaches 1.1 mag (*1, 2, 12*). As a result of the asteroid's weak gravity, no useful constraints on the body's strength can be obtained from the observed topography (*14*).

Craters

The cratering record preserved on the asteroid's surface provides important information on the object's collisional evolution and on the flux of impacting bodies in this part of the asteroid belt. About 60 craters can be identified in Fig. 1; 52 of them are larger than 330 m (about 2 pixels) in diameter. The two largest are about 1.3 and 1.6 km across. Compared with most planetary satellites, Gaspra shows fewer craters per unit area; particularly noteworthy is the absence of intermediate and large craters (2 to 6 km in diameter). For reasons discussed below, the two large concavities seen on the limb (Fig. 1C) probably cannot be considered as craters.

The pixel size of 164 m prevents detailed

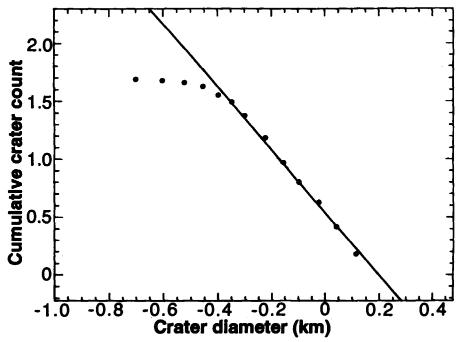

Fig. 5. Cumulative crater frequency versus diameter measurements for Gaspra craters. The data are graphed on a log-log plot. A straight line fit to points for craters 400 m in diameter or larger has a slope of −2.7 with an estimated uncertainty of about ±0.5. See (*19, 24*) for details.

analysis of the morphology of even the largest crater b in Fig. 1B (about 1.6 km in diameter), but several characteristics can be noted. The 1.3-km-diameter crater (a in Fig. 1B displays subtle indications of a raised rim; crater b shows hints of rim segments. We estimated the depth of crater b, which we assume to be a circular crater, by using the aspect ratio of its long and short dimensions to determine incidence and viewing angles. The analysis yields a central depth of about 150 m, which is somewhat shallow for fresh craters of comparable size on other objects. Crater a has a distorted outline, and is not amenable to this type of analysis.

There are no obvious ejecta blankets in this image, and none are expected on asteroids of this size. Few if any topographic expressions of ejecta blankets have been identified on small satellites, although albedo features apparently associated with ejecta have been detected on Phobos and Deimos (*15–17*). The albedo features associated with the ridge crest along which craters g and f (Fig. 1B) are located are similar to bright features on ridges on Phobos and Deimos, some of which are associated with small craters (*15, 18*). A few structural features lie close to prominent craters. Examples include what may be a curved ridge outlined in Fig. 1C close to crater a and a curved depression near crater d (Fig. 1D).

Preliminary crater counts (cumulative) are plotted in Fig. 5. Counts in the diameter range between 0.4 and 1.5 km are most reliable; the measured slope of a power law fit over this diameter range is −2.7 with a likely uncertainty of ±0.5 (*19*). The corresponding slope for a differential or incremental plot is −3.7. This range includes slope values that are similar to, or somewhat steeper than, those considered in the most recent models (*10, 11*). A differential slope of −3.5 is expected for a collisionally relaxed population of impactors (*20*). The standard lunar cratering curve proposed by Neukum *et al.* (*21*) to apply to all solid surfaces in the inner solar system including the asteroids has a differential slope slightly steeper than −4 in the diameter range of observed Gaspra craters.

Because of the relatively low number of craters, we take the observed distribution of crater diameters to be representative of the production function of projectiles reaching Gaspra (~20 m in diameter and larger). There are no other direct observations of the population of main belt asteroids in this size range. Pre-encounter estimates of the numbers of such objects varied by more than four orders of magnitude (*11*). The observed slope of the power law relation supports views that cratering by small objects is an important process in this part of the asteroid belt (*22*). The result is also consistent with the view that the similarly steep distribution for small lunar craters is a reflection of the size distribution of primary impactors and is not a result of secondary craters (*23*).

If the two 8-km features on Gaspra's limb profile are craters, the relative frequency of such giant craters would fall well above the trend suggested by the frequency distribution of the smaller craters. However, it is not likely that craters this large could form on a body as small as Gaspra without disrupting it. The concavities could be giant spall zones caused by impacts that would be expected to have disturbed Gaspra to considerable depth and possibly wiped out records of craters less than a few kilometers across. In such a case, Gaspra's cratering age might be the time since the last such disruptive spallation event.

Collisional and Surface Ages

The Galileo data provide some constraints on models of collisions in Gaspra's part of the asteroid belt. We estimated a relative age for Gaspra's surface by comparing Gaspra's crater population with that of postmare craters on the moon. We calculated production rates for craters across 1 km on the moon and on Gaspra using (i) the known production rate of craters across 10 km on the moon; (ii) the telescopically observed asteroid size distribution (extrapolated conservatively and then augmented at small sizes by a steeper −3.5 differential slope, consistent with both the observed crater distribution on Gaspra and the lunar crater production function); (iii) the intrinsic collision rate for Gaspra; and (iv) strength- or gravity-scaling for rock where appropriate to find ratios of projectile size to crater size. We estimate that the production rate for craters greater than 1 km in diam-

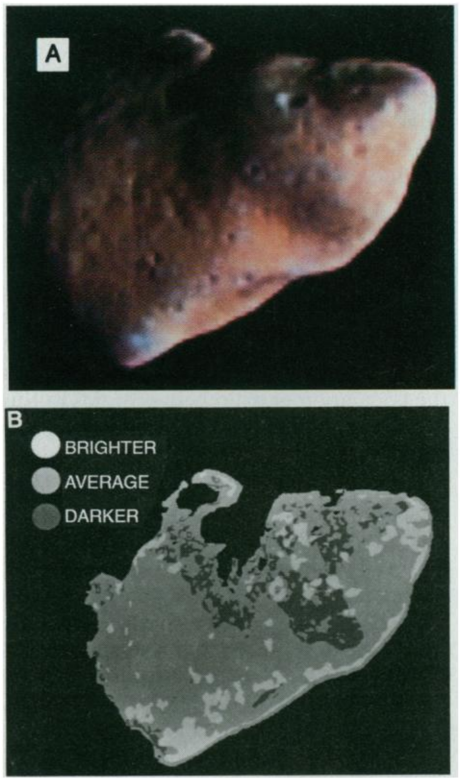

Fig. 6. (**A**) Enhanced color reconstructed from violet, green, and 1-μm images. Color variations are shown much more strongly than they would appear to the human eye, but this presentation provides a valid impression of the spectral variability of areas on Gaspra and of the relation of the color variations with topography. Some ridge areas and areas surrounding certain craters appear bluish in this presentation. Inter-ridge areas (local lows?) are darker and more red. That the observed color differences completely surround some craters demonstrates that these variations are not caused by inadequate removal of local slope effects in the analysis. (**B**) Terrain map showing distribution of three principal units defined on the basis of color-albedo properties (see Table 1 and Fig. 7).

Table 1. Estimated normal albedos of selected materials on Gaspra.

Area	Violet (0.40 μm)	Green (0.56 μm)	Near-infrared (0.89 μm)	1 μm (0.99 μm)
Global mean	0.19 ± 0.04	0.27 ± 0.05	0.29 ± 0.05	0.28 ± 0.03
Brighter	0.21 ± 0.02	0.30 ± 0.03	0.31 ± 0.03	0.29 ± 0.02
Average	0.20 ± 0.03	0.28 ± 0.05	0.30 ± 0.05	0.28 ± 0.05
Darker	0.15 ± 0.02	0.21 ± 0.03	0.23 ± 0.02	0.22 ± 0.03

eter on Gaspra is ~50 times that on the moon (*24, 25*). Observing that Gaspra actually has only three or four times as many 1-km craters as the lunar maria (Fig. 5) and taking the lunar maria to be 3.5 billion years old, we conclude that Gaspra's cratering age is 200 million years (m.y.).

The mean lifetime between catastrophic collisions for an object of Gaspra's size is estimated to be 500 m.y. (*26*). Thus, Gaspra's apparent age is 40% (200 to 500 m.y.) of the expected lifetime of a body its size, and a reasonable assumption is that Gaspra attained its present form through the catastrophic collisional disruption of a precursor body in the Flora region of the asteroid belt.

Gaspra's model lifetime could be as old as many billions of years (dating it back to the epoch of the Late Heavy Bombardment) if the asteroid's interior is much stronger than rock, as could be true if it has the inherent strength of ductile metal. The deduced cratering age could also be correspondingly older if Gaspra has a strong metallic surface. On the other hand, Gaspra's surface could be younger than 200 m.y. if the number of projectiles of several tens of meters size is more numerous than we assumed. The estimates of cratering age and mean lifetime given above are conservative and for the assumption that the asteroid has a rocky composition. No measurements of Gaspra's density are available to constrain its bulk mechanical properties.

Regolith Evolution

On larger bodies ejecta produced during cratering events can lead to the accumulation of significant regoliths. But what about a body as small as Gaspra? Gaspra's surface morphology appears subdued. The ridges that define the asteroid's shape have a smooth appearance reminiscent of bodies with deep fragmental surface layers, or regolith. Many tens of meters of regolith might be required to smooth out surface relief to the degree implied; however, calculations suggest that bodies as small as Gaspra, if made of competent rock, will not retain such depths of regolith (*27, 28*).

It is likely that surface gravity on Gaspra is about 1 cm s^{-2} and that the escape velocity is less than 10 m s^{-1}. Models suggest that Gaspra is sufficiently small that virtually all of its ejecta would escape to space, provided that impacts occur into strong rock or metal. Calculations predict that regoliths will be <1 mm thick for such cases if the surface were originally free of regolith (*29*), but these predictions are uncertain, as there are inadequate experimental data on low-velocity ejecta (few meters per second). Strain-rate scaling of rock suggests that perhaps half the ejecta from the few largest craters on Gaspra might be retained; if so, perhaps a couple meters of regolith could be produced (*30*).

If Gaspra is made of weak, cohesionless material (or had an original blanket of regolith) so that cratering is in the gravity-controlled regime [as in (*27*), applied to the Martian satellites], half or more of the ejecta could be retained from impacts of all scales. By analogy with Phobos and Deimos, perhaps 10 to 20 m of regolith could eventually develop on a weak Gaspra. However, because of its comparatively young cratering age (40% of collisional lifetime), the regolith depths developed to date would be less than half of these depths. Even with 100% ejecta retention, the observed production population of craters on Gaspra (extended to the sides of Gaspra we have not yet seen) can account for only several meters of globally distributed ejecta; we would have to appeal to large craters on the unseen portions of Gaspra to produce enough ejecta volume for a regolith thick enough (many tens of meters) to subdue morphologic features. As discussed in the following section, the distribution of colors and albedo variations on Gaspra suggests that some regolith has been retained. It has also been suggested that Gaspra's softened morphology may be due to erosion caused by the relatively high abundance of small impactors (steep production function), as previously modeled in the lunar context (*31*).

Regolith: Albedos and Color

The surface of Gaspra exhibits subtle, but spatially coherent albedo and color variations (Fig. 6A). We determined colors and albedos from images calibrated using in-flight dark current and preflight radiometric calibration and blemish files (*32, 33*). Accurate measurements of local surface albedos require knowledge of Gaspra's shape to determine local angles of incidence and emission. For this analysis, we used the shape model shown in Fig. 2 (*34*).

Image ratio analysis distinguishes at least three widely distributed materials that correlate spatially with identifiable geological features (Fig. 6, A and B). "Brighter" deposits surround some craters and are characterized by ratios of 1 μm to green radiation about 5% below the global mean. Variegations of similar materials at spatial resolutions too small to reveal possible central craters mottle Gaspra's ridges. A second material, visible as diffuse "darker" regions covering several major interridge facets of Gaspra's surface, is distinguished by ratios of 1 μm to green radiation about 4% above average. By far the most widespread material on Gaspra's surface is intermediate in albedo and color

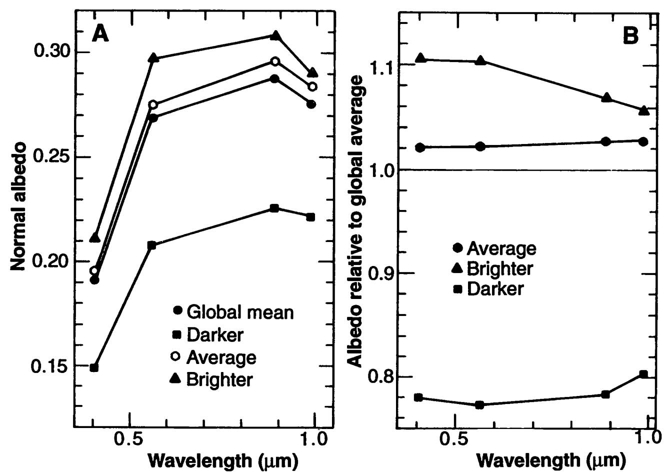

Fig. 7. (**A**) Normal albedos of Gaspra terrains. Our value for the average normal albedo (0.27) for the surface is slightly higher than the 0.2 to 0.22 value for the geometric albedo quoted by Goldader *et al.* (*46*). The difference may reflect remaining uncertainties in the absolute calibration of the SSI camera but could also be explained in part in terms of expected differences between the normal and geometric albedos of S-type asteroids (*34*). (**B**) Gaspra terrain albedos plotted relative to average global values (compare with Table 1). Table 1 lists the calculated average normal albedos of each terrain unit with 1σ standard deviations (*34*). The large (>10%) standard deviations probably result from the wide distribution of actual local slopes around those predicted by our shape model.

and nearly identical to the average global albedo and color of Gaspra. These three materials are labeled "brighter," "darker," and "average" in Fig. 6B.

The unit map of Fig. 6B was used to isolate radiance factors of the three terrain materials, and the corresponding photometric geometries were calculated from the shape model and known directions of the sun and spacecraft. Gaspra's properties are consistent with those of a lunar-like photometric behavior, expected for a surface covered by a relatively dark, highly textured material (35). The observed behavior is consistent with, but does not necessarily require, the presence of an optically thick layer of regolith. Gaspra's albedo is relatively uniform (Table 1); however, variations of some 10 to 20% occur and correlate with the small but definite color variations, as well as with surface morphology. Average materials are only a few percent higher in albedo than Gaspra as a whole and have the same spectral character (Fig. 7), exhibiting a prominent 1-μm absorption attributed to the presence of olivine and, perhaps, pyroxene (36). "Darker" materials are about 20% lower in albedo and exhibit a significantly weaker 1-μm absorption. In contrast, "brighter" materials are about 10% higher in albedo, have a stronger 1-μm absorption, and an overall tendency to be slightly less red. The spectral and albedo properties of "average" materials cannot be modeled by any simple areal mixture of "darker" and "brighter" materials. However, "average" materials may simply be an intimate particle mixture of the "darker" and "brighter" components, or represent a mixture in which at least one of the components has undergone optical alteration. The variations observed on Gaspra are much smaller than differences between rocks and optically mature lunar soils (*37*). The observed color-albedo trends could be related to differences in average particle size (*38*). Another viable explanation is that fresher, more mafic materials are exposed near craters and ridges, perhaps a result of the downhill migration of regolith. Regolith accumulations would occur in the lower, darker areas. Even on irregular bodies, ridges tend to be regions of high gravitational potential, and intervening areas tend to be gravitational lows (*14, 16*). Some minor optical maturation process may be involved, even though it has been argued that such processes should not be effective on asteroid-sized bodies (*27, 39*). Qualitatively, at least, the lower albedo and weaker 1-μm band of dark materials are consistent with shock alteration of chondritic materials (*40*) or an enhanced metallic component (*41*).

Studies of Phobos and Deimos provide a useful basis for interpreting the spatial distribution of albedo and color variations (*15, 17, 18*). Deimos exhibits higher albedos on local highs (ridges), and albedo streamers penetrate into local gravitational lows. These streamers are interpreted as exposures of optically fresher material from the ridges; attendant lateral transport and downslope movement has concentrated the more altered materials in the gravitational lows (*42*). Similar bright materials occur on crater rims on Phobos (*15, 18*). This distribution suggests that a thin surface layer has been removed and an optically different substrate has been exposed (*17*). Similarly, on Gaspra, the materials with the strongest mafic absorptions are located on the ridges, and the materials with the weaker mafic absorptions are on interridge slopes. Downslope movement of altered material, due to thermal creep or to impact-induced erosion and redistribution of regolith, could expose the less optically altered material on ridges.

Other Surface Features

In addition to craters, other surface features are evident in the Galileo images. Although at the limit of resolution, several of the features occur in at least two separate images of the sequence and must therefore be real. Most conspicuous are a number of linear features some 200 to 400 m wide and up to several kilometers long, a few of which are outlined in Fig. 1D. At the available resolution, it is uncertain whether they are trough-like in morphology or whether they represent almost coalescing elongated depressions. They could be similar to grooves seen on Phobos (*43*). If they are grooves, they are likely evidence of nearly catastrophic impacts (*44*). A few of the linear features are distinctly curved. One of these, among the most conspicuous, may be associated with a prominent crater (d in Fig. 1D).

Outstanding Questions

No evidence for any satellite of Gaspra was found in any of the four images. No individual pieces of orbiting debris were evident down to a size limit of 27 m in radius (with Gaspra-like photometric properties). No evidence of any cloud of debris was found. The search covered the region from about 100 to 200 m above Gaspra's surface out to about 10 asteroid radii, only a tiny fraction of the zone of potential dynamical stability estimated by Hamilton and Burns (*45*) to cover a volume of 450 by 450 by 210 asteroid radii. The remaining images stored on the tape recorder will allow examination of a much wider region.

In part for reasons of mission safety, the Galileo flyby distance at Gaspra was too large to allow a determination of the asteroid's mass (*47*). Thus, even after a better volume estimate is obtained after playback of the remaining imaging data, the asteroid's mean density will remain undetermined. The strongest clues to the resolution of the S-asteroid debate might come from the results of searches for marked compositional heterogeneity across the asteroid's surface. Key to this search are the spectral data obtained by the Near Infrared Imaging Spectrometer (NIMS) instrument, most of which remain to be played back. Although of limited spatial resolution, these data, which cover the spectral range between 0.7 and 5.2 μm, can be used to test the compositional homogeneity of Gaspra on scales comparable to about half a hemisphere. The imaging data, although of less detailed spectral resolution, can be used to test for color differences between 0.4 and 1.0 μm on kilometer scales (or better) over most of the asteroid's surface, on the basis of color information obtained by the camera on approach to Gaspra over a whole rotation period of the asteroid. These images, which remain to be played back, will also enable a direct measurement of Gaspra's spin state (pole orientation and spin period) and provide better determinations of the asteroid's overall shape, size, and volume (*49*).

REFERENCES AND NOTES

1. J. D. Goldader *et al.*, *Astron. J.* **102**, 1503 (1991); see also M. DiMartino *et al.*, *Icarus* **87**, 372 (1990); S. Mottola *et al.* (preprint) (1991); W. Wisniewski, personal communication.
2. P. Magnusson *et al.*, *Icarus*, in press.
3. J. Spencer and D. Tholen, personal communication.
4. C. R. Chapman, D. Morrison, B. Zellner, *Icarus* **25**, 104 (1975); J. C. Gradie *et al.*, in *Asteroids II*, R. P. Binzel, T. Gehrels, M. S. Matthews, Eds. (Univ. of Arizona Press, Tucson, 1989), pp. 316–335.
5. D. J. Tholen and M. A. Barucci, in *Asteroids II*, R. P. Binzel, T. Gehrels, M. S. Matthews, Eds. (Univ. of Arizona Press, Tucson, 1989), pp. 298–315.
6. C. R. Chapman, in *Asteroids*, T. Gehrels, Ed. (Univ. of Arizona Press, Tucson, 1979), pp. 25–60; M. J. Gaffey, *Icarus* **60**, 83 (1984); ______, J. F. Bell, D. P. Cruikshank, in *Asteroids II*, R. P. Binzel, T. Gehrels, M. S. Matthews, Eds. (Univ. of Arizona Press, Tucson, 1989), pp. 98–127.
7. C. R. Chapman, paper presented at the Asteroids, Comets, Meteors Conference, Flagstaff, AZ (1991).
8. B. Zellner, D. J. Tholen, E. F. Tedesco, *Icarus* **61**, 355 (1985).
9. G. W. Wetherill, *J. Geophys. Res.* **72**, 2429 (1977).
10. P. Farinella *et al.*, *Lunar Planet. Sci.* **XXII**, 363 (1991); *Astron. Astrophys.*, in press; A. Cellino, V. Zappala, P. Farinella, *Monthly Notices Roy. Astron. Soc.*, in press.
11. N. Namiki and R. P. Binzel, *Geophys. Res. Lett.* **18**, 1155 (1991).
12. A. Harris, personal communication.
13. S. Mottola *et al.*, in preparation.
14. P. C. Thomas, *Icarus* **77**, 248 (1989); T. V. Johnson and T. R. McGetchin, *ibid.* **18**, 612 (1973).
15. J. Veverka and P. Thomas, in *Asteroids*, T. Gehrels, Ed. (Univ. of Arizona Press, Tucson, 1982), pp. 628–654.
16. P. Thomas, J. Veverka, S. Dermott, in *Satellites*, J. Burns and M. S. Matthews, Eds. (Univ. of Arizona Press, Tucson, 1986), pp. 802–835.
17. S. Murchie *et al.*, *J. Geophys. Res.* **96**, 5925 (1991).
18. P. Thomas, *Icarus* **40**, 223 (1979).
19. The data shown are averages of three independent crater counts. A straight line fit to data for craters 400 m or larger yields a slope of −2.7. We estimate that the uncertainty in this determination is about ±0.5.
20. J. S. Dohnanyi, in *Physical Studies of Minor Planets*, T. Gehrels, Ed. (*NASA SP-267*, NASA, Washington, DC, 1971), pp. 263–295.
21. G. Neukum *et al.*, *Proc. Lunar Sci. Conf.* **6**, 2597 (1975).
22. C. R. Chapman *et al.*, *Lunar Planet. Sci.*, in press.
23. G. Neukum *et al.*, *The Moon* **12**, 201 (1975).
24. The production rate of lunar maria craters (>10 km in diameter) is 0.3×10^{-14} km^{-2} yr^{-1} (*23*). Sizes of projectiles to produce 1- and 10-km craters on the moon are obtained from Holsapple Schmidt scaling [J. H. Melosh, *Impact Cratering* (Oxford Univ. Press, Oxford, 1989), p. 245] for competent rock in the gravity regime. There are about 375 times as many lunar maria craters that are >1 km in diameter as there are >10 km in diameter (*23*), yielding a crater production rate (for >1 km craters) of 1.1×10^{-12} km^{-2} yr^{-1}. For Gaspra, we estimate that a projectile 100 m in diameter is needed to form a crater 1 km in diameter at an impact speed of 5.5 km s^{-1} (*10*) into basalt in the strength regime. The asteroid size distribution is based on a conservative extrapolation of the Palomar Leiden Survey (differential slope −2.95) down to the projectile size (175 m) that produces a 2.5-km lunar crater, where the lunar curve turns up, and a differential slope of −3.5 for smaller sizes consistent with the observed range of possible slopes on Gaspra. This relation yields a Gaspra crater production rate (for craters >1 km in diameter) of 5.7×10^{-11} km^{-2} yr^{-1}, which is about 50 times the lunar crater production rate. The result is conservative; the ratio would be higher, and Gaspra's age correspondingly younger, if there are even more small asteroids, which we believe is more likely than there being fewer small asteroids.
25. The counts shown in Fig. 5 correspond to an approximate surface area of 140 km^2.
26. We use the same asteroid size distribution as for the cratering-age calculation and Farinella *et al.*'s (*10*) calculations of Gaspra's intrinsic collision rates with other asteroids, and assume that Gaspra is shattered and disrupted by a projectile 350 m across. Namiki and Binzel (*11*) get younger ages because they attached the steeply sloping power law to the observed asteroid distribution at a larger size.
27. J. Veverka *et al.*, in *Satellites*, J. Burns and M. S. Matthews, Eds. (Univ. of Arizona Press, Tucson, 1986), pp. 342–402.
28. The diameter of a rocky body at which there is a transition between ejecta retention and total ejecta escape is about 70 km. Because of a typographical error, this size was reported as 20 km in (*27*); this value actually applies to icy bodies (K. R. Housen, personal communication).
29. K. R. Housen *et al.*, *Icarus* **39**, 317 (1979); recent calculations by E. Ausphang and M. Nolan [*Lunar Planet. Sci.* **XXIII**, 43 (1991)] provide another view of regolith production on small bodies.
30. K. R. Housen, *Lunar Planet. Sci.* **XXIII**, 555 (1992).
31. C. R. Chapman, *Icarus* **46**, 337 (1968); L. A. Soderblom, *J. Geophys. Res.* **75**, 2655; C. R. Chapman *et al.*, *ibid.*, p. 1445.
32. M. J. S. Belton *et al.*, *Space Sci. Rev.*, in press.
33. This procedure was used because the Gaspra images were the first data taken after removal of the camera aperture cover, and inflight calibration data are not yet available. Except for the 0.89-μm image, the relative broadband whole-disk colors of Gaspra in the calibrated images agree to within 4% of the average spectral properties observed from Earth (*1*). The violet (0.40 μm), green (0.56 μm), near-infrared (0.89 μm), and 1-μm images were multiplied by factors of 1.04, 1.00, 1.16, and 1.03, respectively, to scale them to average Earth-based colors.
34. By definition, the normal albedo, r_n, of a surface is its reflectance at $i = e = \alpha = 0°$, where i, e, and α refer to the angles of incidence, emission, and phase, respectively. To extrapolate measured radiance factors to this geometry, we modeled disk-resolved photometric behavior with a simple lunar-like photometric function (*35*) and used Gaspra's (Earth-based) mean whole-disk phase curve (*1, 2, 12*). The relation of r_n to the geometric albedo p measured by ground-based observers is dependent on the shape of the object and the surface scattering law. For S-type asteroids it is expected that $r_n \geq 1.05p$ (*35*).
35. L. M. French and J. Veverka, *Icarus* **54**, 38 (1983).
36. J. B. Adams, *Science* **159**, 1453 (1968).
37. T. B. McCord *et al.*, *J. Geophys. Res.* **77**, 1349 (1972); T. B. McCord, *ibid.* **74**, 3131 (1969).
38. W. G. Egan *et al.*, *Icarus* **19**, 358 (1973); M. J. Gaffey, thesis, Massachusetts Institute of Technology, Cambridge, MA (1974).
39. D. L. Matson *et al.*, *Proc. Lunar Sci. Conf.* **8**, 1001 (1977).
40. D. T. Britt and C. M. Pieters, *Lunar Planet. Sci.* **XXI**, 127 (1990).
41. E. A. Cloutis *et al.*, *J. Geophys. Res.* **95**, 8233 (1990).
42. P. Thomas and J. Veverka, *Icarus* **42**, 234 (1980).
43. P. Thomas *et al.*, *J. Geophys. Res.* **84**, 8457 (1979).
44. P. Thomas and J. Veverka, *Icarus* **40**, 394 (1979).
45. D. Hamilton and J. Burns, *ibid.* **92**, 118 (1991).
46. J. D. Goldader, *Bull. Am. Astron. Soc.* **23**, 1142 (1991).
47. J. D. Anderson, personal communication.
48. R. L. Millis and D. W. Dunham, in *Asteroids II*, R. P. Binzel, T. Gehrels, M. S. Matthews, Eds. (Univ. of Arizona Press, Tucson, 1989), pp. 148–170.

49. This contribution is dedicated to the memory of C. Yeates. We acknowledge the assistance of numerous individuals, in particular the Galileo Flight Team led by W. O'Neil, N. Ausman, and M. Landano and the Galileo Navigation Team, and the SSI support staff at JPL, including H. Breneman, A. Harch, C. Heffernan, B. Paczkowski, and B. Roman. We also thank B. Carcich and L. Wainio's group at MIPS and the many colleagues who shared the results of their ground-based telescopic observations and analyses with us, including M. Barucci, R. Binzel, B. E. Clark, D. R. Davis, J. D. Goldader, W. Golish, M. Gonano-Brewer, A. Harris, T. Herbst, S. Howell, R. Kirk, C. D. Madras, P. Magnusson, S. Mottola, M. Robinson, J. Spencer, D. Tholen, and W. Wisniewski, and also D. Hall and J. Rahe for coordinating the efforts to obtain supporting observations. D. Tholen, S. Dermott, and an anonymous reviewer provided helpful comments on the original version of this contribution. A portion of the research was carried out by the Jet Propulsion Laboratory, California Institute of Technology, under contract with NASA. The National Optical Astronomy Observatories are operated by the Association of Universities for Research in Astronomy, Inc. (AURA), under cooperative agreement with the National Science Foundation.